Algebraic Damping of Diocotron Waves by a Flux of Particles Through the Wave Resonant Layer

Andrey A. Kabantsev, Thomas M. O'Neil, and C. Fred Driscoll

Department of Physics, University of California at San Diego, La Jolla, CA USA 92093-0319

Abstract. Pure electron plasma experiments characterize a novel form of *algebraic* diocotron mode damping, distinct from the usual exponential damping. This algebraic damping occurs when trap asymmetries cause a weak outward particle flux $\Gamma(r)$ through the diocotron mode resonant radius r_m. The $m = 1$ and $m = 2$ diocotron mode amplitudes are each observed to decay as $d(t) = d(t_*) - \gamma \cdot (t - t^*)$, where t_* is the time at which the outward particle flux reaches r_m. Moreover, with appropriate amplitude normalization, we find that $\gamma \sim \Gamma$. A theory model based on conservation of momentum agrees qualitatively with experiments, but some aspects remain puzzling.

Keywords: nonneutral plasma, diocotron modes, damping
PACS: 52.27.Jt, 52.35.-g, 52.35.Fp, 52.25.Fi

The study of diocotron modes has a venerable history dating back more than a half century to early work on magnetrons and hollow electron beams [1–4]. More recently, these modes have proven to be dominant features in the low frequency dynamics of nonneutral plasmas in long cylindrical Penning-Malmberg traps and toroidal traps [5–13]. In shorter hyperbolic traps, spheroidal charge clouds exhibit analogous center-of-mass "magnetron" and higher-order shape-distortion modes [14].

For the longish Penning-Malmberg traps considered here, exponential diocotron mode growth can be caused by a non-monotonic plasma density profile [5]; by a resistive boundary wall [15]; and by the axial transit of oppositely-charged particles [16]. In contrast, exponential diocotron mode damping may be caused by electron-neutral collisions [11]; by a spatial Landau resonance [17]; by negative resistance (feedback) on the wall; by plasma viscosity acting on length changes due to rotational pumping [18] or magnetic pumping [19]; and by z-kinetic dissipative effects at an internal plasma separatrix [20]. These processes all evolve *exponentially* with time, as $d(t) = d_0 \exp\{\pm\gamma_e t\}$.

Here, we observe a novel *algebraic* damping of the $m = 1$ and $m = 2$ diocotron modes, which occurs when trap imperfections cause a weak flux of particles through the mode's resonant radius. For $m = 1$, the mode amplitude $d \equiv D/R_W$ (off-axis column displacement D normalized by the wall radius R_w) is observed to decrease in time as

$$d(t) = d(t_*) - \gamma_1 (t - t_*) \tag{1}$$

as soon as $(t \geq t_*)$ there is a flux of particles Γ to the cylindrical wall, with $\gamma_1 \propto \Gamma$. The algebraic damping seems to be due to a "one-sided" spatial Landau resonance at $r = R_W$.

In general, the spatial Landau resonance for a mode with frequency f_m occurs at a radius r_m defined by $f_m = m f_E(r_m)$, where f_E is the plasma drift-rotation rate. For $m = 1$ with $r_1 \approx R_W$, algebraic damping is observed only after some plasma particles

have expanded out to the wall. For $m = 2$ with $r_2 = 1.9$ cm $\gtrsim R_p$, the initial condition may have non-zero plasma density $n(r_2)$, in which case exponential damping and/or trapping-induced amplitude oscillations are observed. However, when an initial density profile is created with $n(r_2) = 0$, then there is no exponential damping, and experiments show *algebraic* damping once weak transport processes generates a flux $\Gamma(r_2)$ through the resonant radius.

As adjunct to the damping measurements, we note that the $m = 1$ diocotron mode *frequency* is a sensitive diagnostic of plasma temperature and mean radius changes. Supported by finite-length and finite-amplitude theory, the mode frequency shifts give a self-consistent picture of the plasma evolution.

CORE PLASMA AND HALO FLUX

The experiments utilize a cylindrical Penning-Malmberg trap to confine quiescent, low-collisionality pure electron plasmas. Electrons are confined radially by a nominally uniform axial magnetic field $B = 12$ kG; and are confined axially by voltages $V_c = -100$ V on end cylinders of radius $R_W = 3.5$ cm. The electron columns have length $L_p = 49$ cm, and radial density profile $n(r)$ with central density $n_0 \approx 1.6 \times 10^7$ cm^{-3} and line density $N_L = \pi R_p^2 n_0 \approx 6.1 \times 10^7$ cm^{-1}. The unneutralized charge results in an equilibrium potential energy $\Phi_e(r)$ with $\Phi_{e0} \approx +28$ eV at $r = 0$. This gives an $E \times B$ rotation frequency $f_E(r)$ which decreases monotonically from $f_{E0} \approx 20$ kHz.

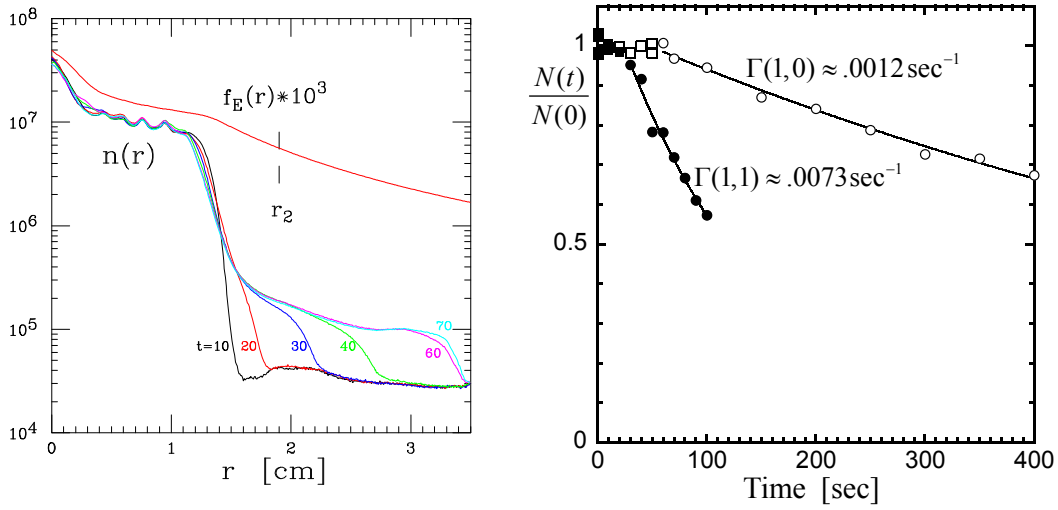

FIGURE 1. (Left) Measured density profile $n(r)$ and calculated $f_E(r)$ at 6 times, as a low-density halo propagates to the wall, driven by a magnetic tilt of $\varepsilon_B = 1$ mRad. The small ripples at 10^7 are an artifact of a phospor burn, and the baseline at 3×10^4 represents background signal. The central ($r \leq 0.2$ cm) clump is typical at these high fields, but negligible for our purposes.

FIGURE 2. (Right) Measured number of particles remaining at late times with a 1 mRad tilt, with and without an additional quadrupole V_{a2}.

The bulk electrons have a near-Maxwellian velocity distribution with an initial thermal energy $T \lesssim 1$ eV. At 12 kG, the cyclotron cooling time for electrons $\tau_c \simeq 2.7$ sec, so

in about 10 sec the bulk electrons cool down to a room (wall) temperature $T \simeq 0.03$ eV. Typical $e-e$ collision frequency in the bulk at this temperature $\nu_{ee} \approx 2 \cdot 10^4$ sec$^{-1} \approx f_{E0}$. Diocotron mode frequencies are $f_1 \simeq 2$ kHz and $f_2 \approx 15$ kHz.

From this cold plasma core, we generate a weak outward flux

$$\Gamma(r) \equiv -\frac{\frac{d}{dt}N_L(r)}{N_L(r)}$$

and a consequent low density "halo" of particles $n_h(r)$ which propagates outward on a 20–100 second timescale. To control this flux, we apply a tilted magnetic field, $\varepsilon_B \equiv B_\perp/B_\parallel \sim 10^{-3}$, or a quadrupole electrostatic asymmetry $V_{a2} \sim 1$ V to one of the sectored confinement cylinders, or both at once [20]. The quadrupole asymmetry is preferable here, as it does not change the original plasma alignment, and thus does not produce an offset to the $m = 1$ diocotron mode.

Figure 1 shows a late-time evolution of plasma density profile $n(r)$ obtained with an applied tilt of $\varepsilon_B \approx 1$ mrad. In the first ten seconds, as bulk electrons cool down to ridigity $R \equiv f_b/f_E \gtrsim 1$, a low-density halo is formed outside of the bulk plasma, which then propagates slowly to the wall. Here, the halo reaches the wall at about 50 sec, and after that its shape remains nearly constant while transporting particles from the bulk plasma boundary to the wall. The flux estimate based on this halo propagation gives $\Gamma \approx 1.2 \cdot 10^{-3}$ sec^{-1}.

Figure 2 shows examples of more accurate measurements of the loss rate $\Gamma[\varepsilon_B, V_{a2}]$ taken by varying shot-to-shot confinement time well beyond the wall touch time $t_*[\varepsilon_B, V_{a2}]$. Here, the open symbols show the normalized total number of confined electrons consecutively dumped to the CCD detector with no $m = 2$ asymmetry applied ($\varepsilon_B = 1$ mrad, $V_{a2} = 0$). This case is consistent with Fig. 1. The closed symbols show evolution of the total number of confined electrons for ($\varepsilon_B = 1$ mrad, $V_{a2} = 1$V) case, when the loss rate Γ is increased manyfold.

$m = 1$ FREQUENCY SHIFTS

Figure 3 shows a typical evolution of the $m = 1$ diocotron mode frequency $f_1(t)$ and amplitude $d_1(t)$ evolution. While the mode amplitude stays nearly constant before the halo touches the wall, the frequency evolution has four generic parts (from I to IV), which can be classified on the base of different terms in the finite-length diocotron frequency expression [21, 22], given by

$$f_1 = \frac{ceN_L(t)}{\pi B R_W^2}\left\{1 + \frac{R_W}{L_p}\left[1.20\left(\frac{1}{4} + \ln\frac{R_W}{R_p(t)} + \frac{T(t)}{e^2 N_L}\right) - 0.671\right]\right\}[1 + \sigma d^2]. \quad (2)$$

Here, the end confinement fields contribute a "magnetron-like" frequency increase proportional to the plasma electrostatic and thermal pressures. The finite amplitude [22] corrections σd^2 are generally negligible for $d \lesssim 10^{-2}$. For $t \lesssim 1$ sec of plasma confinement, there is some (small) increase of the mode frequency due to collisional relaxation of (the partially beam-like) initial velocity distribution (I), including some ionization

of the background gas. However, in short order this peak dives into exponential decline due to cyclotron cooling [23] of electrons from ~ 1 eV to $T_{\rm wall} \sim 25$ meV, as $\Delta T(t) \approx \Delta T(0)\, e^{-t/\tau_c}$ (II).

When the electron temperature gets close to $T_{\rm wall}$, this exponential dive levels off, leaving only a slow linear frequency decrease due to the R_p increase as the halo expands to the wall (III). Finally, when the halo touches the wall at $t = t_*$ (stage IV), the plasma column starts losing particles, and the main term $(d/dt)\ \ln f_1 = (d/dt)\ \ln N_L \equiv -\Gamma$ comes into play. We note that Eq. (2) necessarily needs modification when the plasma extends to R_W.

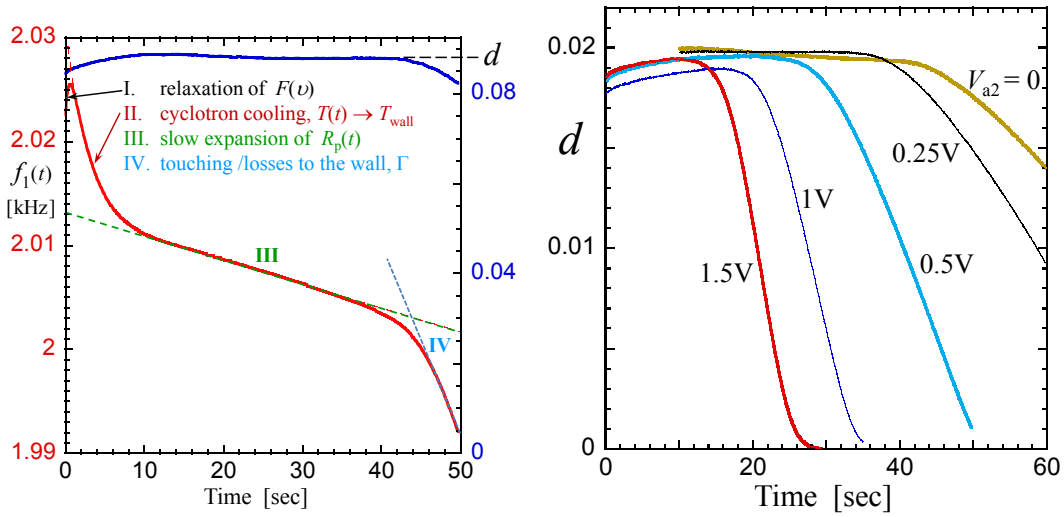

FIGURE 3. (Left) Measured diocotron frequency $f_1(t)$ and amplitude $d(t)$, showing four phases of frequency shifts ($V_{a2} = 0$ case).

FIGURE 4. (Right) Measured diocotron amplitude $d(t)$, showing a varying onset time and varying rate for algebraic damping, as the controlled V_{a2} causes more rapid transport to the wall.

$m = 1$ ALGEBRAIC DAMPING

Figure 4 shows examples of the mode amplitude evolution $d(t)$ for various strengths of applied asymmetry V_{a2}. Note that the amplitudes $d(t)$ remain nearly constant during the $f_1(t)$ frequency evolution stages I, II and III. However, as soon as the halo touches the wall (stage IV), a fast *linear* decline (*algebraic damping*) $d(t) = d(t_*) - \gamma_1 \cdot (t - t_*)$ is observed over two orders of magnitude. Note that although in general the amplitudes of the wall signals shown in Fig. 4 are proportional to the product of $N_L \cdot d$, here the losses in N_L are negligible ($<3\%$) during the time needed to wipe out these small $d \leq 0.02$ modes.

By repeating these procedures at several applied V_{a2} we obtain the set of points γ_1 versus Γ shown in Fig. 5. These points give a linear fit for the *algebraic* damping rate $\gamma(\Gamma) \approx \Gamma$. Thus, the observed *algebraic* damping rate γ of the fundamental diocotron mode is closely proportional to the particle loss rate Γ.

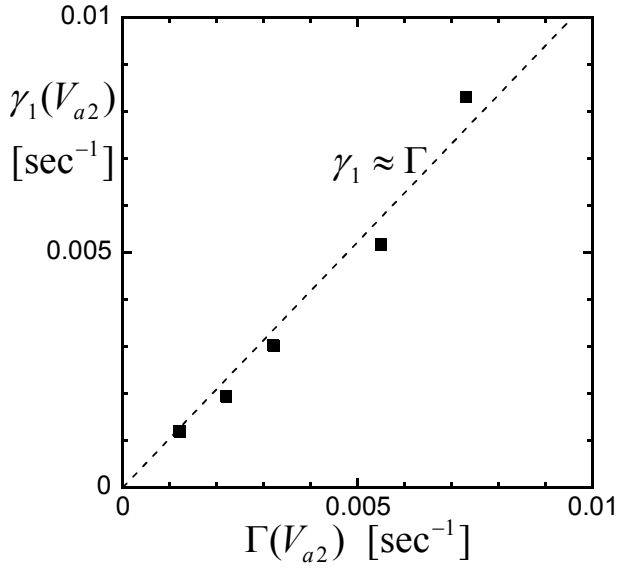

FIGURE 5. Algebraic damping rate γ_1 versus flux rate Γ, where Γ is controlled by V_{a2}.

For modes excited in the beginning of the confinement cycle, the algebraic damping occurs only after the plasma halo reaches $R_{\rm wall}$, and this may introduce some additional uncertainty if the transport rate changes with time. To obtain the damping rate $\gamma_1(\Gamma)$ regardless of corresponding halo-wall contact time, we have excited the diocotron waves at $t_1 = 100$ sec, i.e., when the halo has already touched the wall even in the best aligned plasma column case. Moreover, we restrict our measurements of the wave evolution time to a 25 sec window. This window is long enough to observe complete damping of small amplitude waves ($d \lesssim 0.02$); but complete damping of waves with moderate initial amplitudes ($d \sim 0.1$) would require a 100 sec window, possibly accompanied by significant change in plasma parameters.

Figure 6 shows the damping of several $m = 1$ waves launched at $t = 100$ sec with different initial amplitudes d_0. All these different shots are well fitted by the same damping rate $\gamma_1 \simeq 1.2 \cdot 10^{-3}$ sec^{-1} as $d(t) = d_0 - \gamma_1 \cdot (t - 100)$. Damping of the smallest wave from Fig. 6 is also shown separately in Fig. 7 to illustrate the precision of its linear decrease. Overall, Figs. 6 and 7 demonstrate alegbraic damping over two orders of magnitude in d, spanning $0.001 \leq d \leq 0.1$.

$m = 2$ ALGEBRAIC DAMPING

Surprisingly, we have observed similar (linear-in-time) algebraic damping for $m = 2$ diocotron waves as well. Figure 8 shows the evolution of the $m = 2$ mode amplitude $q_2(t)$ after the expanding halo reaches the $m = 2$ resonant layer at $t = 20$ sec. The linear damping is observed over a 10-fold drop in the plasma quadrupole moment $q_2(t) = q_2(t_*) - \gamma_2 \cdot (t - t_*)$. Figure 9 shows this algebraic damping of the $m = 2$ mode versus tilt angle ε_B, with ε_B determing Γ. Taking a series of such evolutions, we find that

$$q_2(t) = q_2(t_*) - \gamma_2 \cdot (t - t_*)\,, \quad \text{with} \quad \gamma_2 \approx 6\Gamma. \tag{3}$$

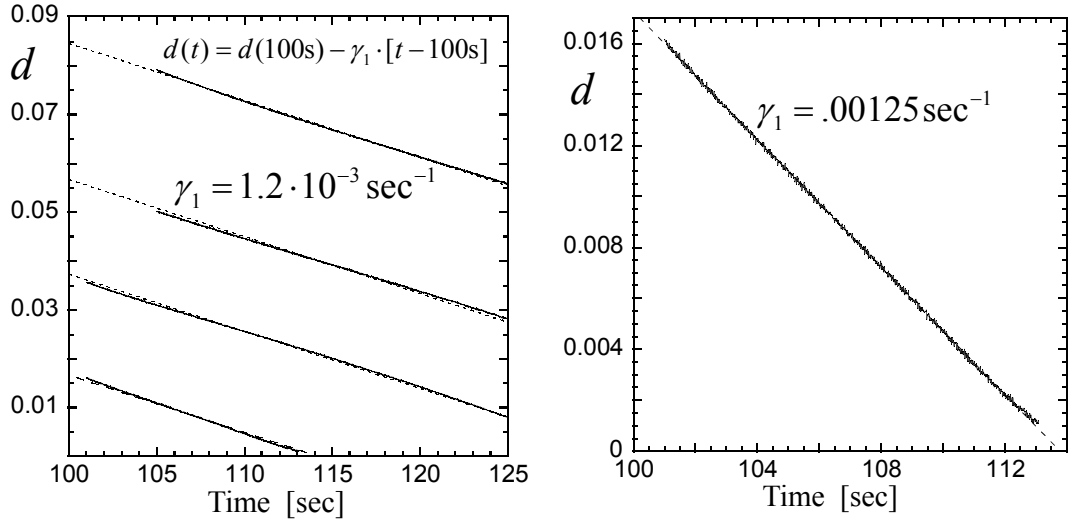

FIGURE 6. (Left) Four measured diocotron amplitude evolutions $d(t)$ showing algebraic damping. The waves are launched at different amplitudes at $t = 100$ sec, i.e. after the halo has contacted the wall.

FIGURE 7. (Right) Measured diocotron amplitude $d(t)$ for the smallest wave in Fig. 6, showing damping which is accurately linear in time even for $d \lesssim 10^{-3}$.

It is instructive to note here that if we change the $m = 2$ metric from the quadrupole moment q_2 to the wall-radius-normalized "displacement" of the plasma edge

$$d_2 \equiv \frac{D_2}{R_W} \equiv q_2 \frac{R_p}{2R_W} \simeq \frac{q_2}{6}, \tag{4}$$

then we obtain

$$d_2(t) = d_2(t_*) - \tilde{\gamma}_2 \cdot (t - t_*)\,, \;\; \text{with} \;\; \tilde{\gamma}_2 \approx 0.5\Gamma. \tag{5}$$

Unlike exponential damping rates, algebraic damping rates vary with parameter normalizations, and the most "theoretically natural" normalization is yet to be decided.

CONCLUSIONS

In conclusion, the linear-in-time algebraic damping of both $m = 1$ and $m = 2$ diocotron modes has been observed in our experiments. This damping begins when an outward flux of particles reaches the spatial Landau resonant radius r_m, and the flux is directly proportional to the particle flux Γ through the resonant layer.

For the $m = 1$ diocotron mode, this resonant radius coincides with the cylindrical wall, so the flux rate Γ is equivalent to the particle loss rate (d/dt) ln N_L. Here, the observed linear-in-time damping seems to be a quite natural result of simple models based on conservation of angular momentum. For the $m = 2$ diocotron waves this linear-in-time damping is somewhat surprising, since the resonant layer trapping width scales as $q_2^{1/2}$. These models are currently being developed, and compared to simulations and experiments.

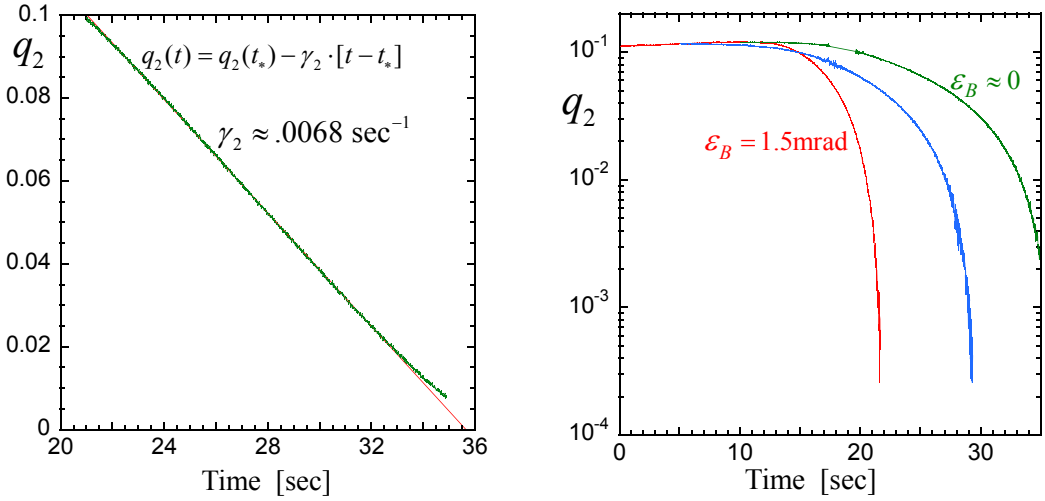

FIGURE 8. (Left) Measured amplitude $q_2(t)$ of the $m = 2$ diocotron mode, showing the same algebraic damping $-\gamma_2 t$ for times after the halo flux has reached the resonant radius r_2.

FIGURE 9. (Right) Measured amplitude $q_2(t)$ for three different magnetic tilts, showing different onset times and different (non-exponential) damping rates.

ACKNOWLEDGMENTS

This work was supported by National Science Foundation Grant No. PHY0903877 and Department of Energy Grant DE-SC0002451.

REFERENCES

1. H. F. Webster, J. Appl. Phys. **26**, 1386 (1955).
2. R. J. Briggs, J. D. Daugherty, and R. H. Levy, Phys. Fluids **13**, 421 (1970).
3. R. C. Davidson, *Theory of Nonneutral Plasmas* (Benjamin, Reading, MA, 1974), Sec. 2.10.
4. R. L. Panton, *Incompressible Flow* (Wiley-Interscience, New York, 1984), Chap. 22.
5. C. F. Driscoll and K. S. Fine, Phys. Fluids B **2**, 1359 (1990).
6. G. Rosenthal, G.Dimonte, and A. Y. Wong, Phys. Fluids **30**, 3257 (1987).
7. A. J. Peurrung and J. Fajans, Phys. Fluids A **5**, 493 (1993).
8. G. W. Hart, Phys. Fluids B **3**, 2987 (1991).
9. R. L. Spencer and S. N. Rasband, Phys. Plasmas **4**, 54 (1997).
10. D. L. Eggleston, Phys. Plas. **1**, 3850 (1994).
11. E. H. Chao, S. F. Paul, and R. C. Davidson, J. Vac. Sci. Tech. A **17**, 2034 (1999).
12. M. R. Stoneking, J. P. Marler, B. N. Ha, and J. Smoniewski, Phys. Plas. **16**, 055708 (2009).
13. Q. R. Marksteiner, T. S. Pedersen, J. W. Berkery, M. S. Hahn, J. M. Mendez, B. Durand de Gevigney, and H. Himura, Phys. Rev. Lett. **100**, 056002 (2008).
14. J. J. Bollinger, D. J. Heinzen, F. L. Moore, W. M. Itano, D. J. Wineland, and D. H. E. Dubin, Phys. Rev. A **48**, 525 (1993).
15. W. D. White, J. H. Malmberg, and C. F. Driscoll, Phys. Rev. Lett. **49**, 1822 (1982).
16. A. A. Kabantsev and C. F. Driscoll, Trans. Fus. Sci. Tech. **51** (2T), 96 (2007).
17. D. A. Schecter, D. H. E. Dubin, A. C. Cass, C. F. Driscoll, I. M. Lansky, and T. M. O'Neil, Phys. Fluids **12**, 2397 (2000).
18. B. P. Cluggish and C. F. Driscoll, Phys. Rev. Lett. **74**, 4213 (1995).

19. S. M. Crooks and T. M. O'Neil, Phys. Plasmas **3**, 2533 (1996).
20. A. A. Kabantsev, D. H. E. Dubin, C. F. Driscoll, and Yu. A. Tsidulko, Phys. Rev. Lett. **105**, 205001 (2010).
21. K. S. Fine and C. F. Driscoll, Phys. Plasmas **5**, 601 (1998).
22. K. S. Fine, C. F. Driscoll, and J. H. Malmberg, Phys. Rev. Lett. **63**, 2232 (1989).
23. T. M. O'Neil, Phys. Fluids **23**, 725 (1980).